IEICE TRANS. INF. & SYST., VOL.E86–D, NO.9 SEPTEMBER 2003

PAPER

EEG Cortical Potential Imaging of Brain Electrical Activity by means of Parametric Projection Filters

Junichi HORI[†*], *Regular Member and* **Bin HE**[†], *Nonmember*

SUMMARY The objective of this study was to explore suitable spatial filters for inverse estimation of cortical potentials from the scalp electroencephalogram. The effect of incorporating noise covariance into inverse procedures was examined by computer simulations. The parametric projection filter, which allows inverse estimation with the presence of information on the noise covariance, was applied to an inhomogeneous three-concentric-sphere model under various noise conditions in order to estimate the cortical potentials from the scalp potentials. The present simulation results suggest that incorporation of information on the noise covariance allows better estimation of cortical potentials, than inverse solutions without knowledge about the noise covariance, when the correlation between the signal and noise is low. The method for determining the optimum regularization parameter, which can be applied for parametric inverse techniques, is also discussed.

key words: *high resolution EEG, cortical potential imaging, inverse problem, parametric projection filter, non-uniform noise, noise covariance*

1. Introduction

Brain electrical activity is spatially distributed over three dimensions of the brain and evolves in time. Electroencephalography (EEG) has historically been a useful modality to provide high temporal resolution regarding the underlying brain electrical activity. However, the spatial resolution of EEG is limited due to the smearing effect of the head volume conductor [1]. In the past decades, much effort has been made in the development of high-resolution EEG techniques, which attempt to map and image spatially distributed brain electrical activity with substantially improved spatial resolution. In parallel to the success of dipole localization methods, in which brain electrical activity is modeled by a few point current dipoles [2]–[9], of interest is the recent develop of EEG spatial enhancement modalities without *ad hoc* assumption on the number of source dipoles. The unique feature of the spatial enhancement approach is its applicability to all kinds of brain electrical sources, thus having the potential of achieving our ultimate goal of imaging brain electric activity.

Of particular interest is the recent development of cortical imaging approaches, in which an explicit biophysical model of the passive conducting properties of a head is used to deconvolve a measured scalp potential distribution into a distribution of electrical potential or current source on the cortical surface. In the cortical current source imaging, an equivalent current source distribution is directly estimated from the scalp potentials [10]–[15]. Such cortical current source imaging approach provides information that may be directly related to the cortical sources [10]. Another approach is to estimate and image the cortical potentials from the scalp recorded potentials [16]–[27]. Because the cortical-potential distribution can be experimentally measured [20], [28], [29] and compared to the inverse imaging results, the cortical-potential imaging approach is also of physiologic importance.

The cortical potential imaging approach has been explored by several investigators. In 1990 Sidman et al. reported an early work on cortical potential imaging, in which they used a hemisphere equivalent dipole layer, to generate an inward harmonic potential function in a homogeneous sphere head volume conductor model, and then reconstruct the potential at an image surface, including the cortical surface [16], [17]. This approach, in which an intermediate dipole layer is used to equivalently represent brain electric sources, has been later extended by He and co-workers to a three-concentric-spheres inhomogeneous head model [22], [24], [30], and shown to be useful in analyzing cognitive activities in a group of subjects without measuring exact head geometry through MRI [27]. Babiloni et al. further extended this approach to a realistically shaped inhomogeneous boundary element head model based subjects' MRI images in which a dipole layer of 364 radially-oriented equivalent current dipoles is embedded. They demonstrated the excellent performance of their technique in both computer simulation studies and in imaging cortical sources of human movement-related and somatosensory-evoked potentials [23]. Gevins and co-workers [19], [20] have been successful in their early work on the brain deblurring, in which potentials at the superficial cerebral cortical surface are estimated from EEG recordings on the scalp using a finite element model of each subject's scalp, skull and cortical surface constructed from their magnetic resonance images. In this method, Poisson's equation is applied to a conducting volume between the scalp and the cortical surface,

Manuscript received October 7, 2002.
Manuscript revised March 31, 2003.

[†]The authors are with the Dept. of Bioengineering, University of Illinois at Chicago, IL 60607, USA.
[*]Presently, with Dept. of Biocybernetics, Niigata University.

and finite element method is used to handle the complex geometry and varying conductivity of the head. Reported predictions of cortical potentials are quite accurate in the cases shown and dramatic improvement in spatial resolution is achieved. Srebro et al. linked the evoked potential field on the scalp with the brain surface field by Green's second identity [18]. The volume conductivity between the surfaces is assumed to be homogeneous and detailed anatomical information for each subject is obtained from MR images. Regularized inversion is applied to get the cortical surface potential estimation. Their physical and human experiments demonstrate that the estimated cortical potential fields are more focused than their scalp field counterparts and could also provide useful information for localizing cortical activity from VEP scalp fields. He and co-workers recently developed a boundary element method based cortical potential imaging technique, in which both the realistic geometry and the inhomogeneity of the head can be taken into account [26], and validated it by comparing with directly-recorded cortical potentials [29].

In parallel to the development of physical models for cortical potential imaging described above, the inverse regularization algorithm plays an important role in cortical imaging. As inherited in any inverse problems, the cortical potential imaging inverse problem is ill-posed, that small perturbation would cause large error in the inverse solutions. Therefore, regularization strategies, such as general inverse with truncated singular value decomposition (TSVD), constrained least square method, and Tikhonov regularization method (TKNV), have been used to solve the ill-conditioned cortical imaging inverse problem. Furthermore, weighted minimum norm solutions have been explored to improve the accuracy of the minimum norm solution [31]–[34]. Of representative is the work of Pascual-Marqui on LORETA [33], [34], which is essentially a Laplacian-weighted minimum norm solution.

Several investigators have further explored the use of advanced regularization methods to improve the cortical imaging inverse results. Dale and Sereno solved the brain inverse problem of estimating the distribution of dipole strengths over the cortical surface by combining EEG and MEG with MRI cortical surface reconstruction [10]. They developed a framework of using source and sensor covariance in order to constraint the underdetermined inverse problem in addition to anatomical constraints extracted from MRI information. However, they did not consider non-white sensor noise in their simulation studies. Sekihara and Scholz proposed the use of Wiener reconstruction of bioelectric current distribution using signal and noise covariance but also assumed uncorrelated Gaussian noise in their model studies [35]. Philips et al. developed a Bayesian framework for image estimation from MEG and a MAP (maximum a posteriori) reconstruction algorithm [11], to estimate focal neural sources. They introduced a priori distribution on the source, which was used to resolve the ambiguities inherent in the inverse problem. While Philips et al. derived a unified framework on the inverse solution including the signal and noise covariance, no investigation was made on evaluating the effect of noise covariance for various source-noise distributions. A comprehensive review was given by Grave de Peralta Menendez and Gonzalez on brain electromagnetic inverse methods using the metrics associated with the measurement space and the source space [12]. The metric for the solution space was discussed in detail comparing with previously proposed methods such as LORETA [33]. We have recently developed a parametric projection filter based algorithm for cortical current dipole imaging [14], and demonstrated the advantages of taking the noise covariance into consideration. These works demonstrate the importance of taking into account the statistical characteristics of signal and noise, in estimating brain electric activity.

In the present study, we hypothesize that a regularization approach incorporating information about noise covariance alone would improve the restorability of cortical potentials from scalp potentials, meanwhile eliminating the difficulty of estimating signal covariance. Since the noise covariance is not difficult to obtain from pre-stimulus evoked potentials, the noise-covariance approach would provide an easy-to-implement yet taking into consideration of the statistical properties of measurement noise. We have tested this approach in the present study through a series of computer simulations.

2. Method

2.1 Principles of Cortical Potential Imaging

The physical model of the cortical potential imaging used in the present study was initially proposed by Sidman et al. [16], [17] and improved by He and Coworkers [22], [24], [30]. A brief description on the approach we used in this study follows. The head volume conductor is approximated by the inhomogeneous three-concentric-sphere model. This head model takes the variation in conductivity of different tissues, such as the scalp, the skull and the brain, into consideration. A hypothetical dipole layer is assumed within the brain sphere being concentric to the cortical surface. Radial current dipoles are uniformly distributed over the spherical dipole layer to simulate brain electrical sources accounting for the scalp potentials. The transfer function from the dipole layer to the scalp potentials is obtained by considering the geometry of the model and physical relationship between the quantities involved. The strength of the dipole layer is estimated from the scalp potentials. The potential field at the surface of the brain (cortical surface) is then reconstructed by solving the forward problem from the equivalent dipole layer to cortical potentials.

The observation system of brain electrical activity on the scalp shall be defined by the following equation:

$$g = Af + n \tag{1}$$

where f is the vector of the equivalent source distribution of a dipole layer, n is the vector of the additive noise and γ is the vector of scalp-recorded potentials. A represents the transfer matrix from the equivalent source to the scalp potentials. In the present approach, f is the strength of the dipole layer. It is important to infer the origins from the scalp-recorded EEG, and to localize the sources that generate the observed EEG on the scalp. The inverse process shall be defined by

$$f_0 = Bg \tag{2}$$

where B is the restoration filter and f_0 is the estimated source distribution of the dipole layer. As the number of measurement electrodes is always smaller than the dimension of the unknown vector f, this problem is an underdetermined inverse problem. The details of the restoration filter B are shown in Sect. 2.2. Once the dipole moments are estimated, the potential distribution, h_0, on the cortical surface can be calculated through forward solution:

$$h_0 = Cf_0 \tag{3}$$

where C is the transfer matrix from the equivalent dipole layer to the cortical potentials. Thus, the cortical potential is reconstructed from the scalp measurements, through an intermediate dipole layer. In the next section, we consider how to decide the optimum restoration filter, B for cortical potential imaging.

2.2 Inverse Techniques

The pseudoinverse filter, denoted by A^+, minimizes the norm of restored dipole layer distribution f_0 under the constraint

$$g = Af_0 \tag{4}$$

in the absence of noise. In practice, singular value decomposition (SVD) can be used to calculate A^+ [36], [37]. In the presence of noise, the truncated SVD is implemented in order to reduce the effect of noise [38]. Moreover, Tikhonov regularization method [39] is also used, which leads to

$$B = (A^*A + \gamma I)^{-1}A^* \tag{5}$$

with γ a small positive number known as the regularization parameter, I the identity matrix and A^* the transpose matrix of A. The constrained least-squares filter minimizes some quadratic functional of f_0, defined by $||Df_0||^2$, under the constraint

$$||g - Af_0||^2 = E||n||^2 \tag{6}$$

with $||\cdot||$ the norm in the Hilbert space and E the expectation [40]. This leads to the restoration filter

$$B = (A^*A + \gamma D^*D)^{-1}A^*. \tag{7}$$

If $D = I$, then Eq. (7) is reduced to the regularized pseudoinverse filter (Eq. (5)). If $D = R^{-1/2}Q^{1/2}$with R and Q the signal and noise covariance, respectively, then Eq. (7) is reduced to the parametric Wiener filter (PWF) [41], [42]. However, it is difficult to obtain the signal covariance and even if the signal covariance is obtained, the filter may not provide satisfactory performance for abnormal signals, which is obviously different from the expectation of signals.

In order to overcome this problem, the projection filter has been introduced to solve the inverse problem [41], [42]. The projection filter is a method, which allows to estimate solutions in presence of information on noise covariance structure. In the present study, we use the projection filter to achieve the inverse estimation for cortical imaging.

Let P be the orthogonal projection operator onto the range of A^*. The projection filter criterion becomes: find out all operators B, which minimize the noise component

$$E||f_0 - Pf||^2 = E||B_n||^2 = tr(BQB^*) \tag{8}$$

subject to

$$BA = P \tag{9}$$

where E in Eq. (8) is the expectation over the noise $\{n\}$ ensemble and $tr(\cdot)$ is the trace of an operator. In the case of a nonsingular noise covariance Q, the projection filter is derived by

$$B = (A^*Q^{-1}A)^+A^*Q^{-1}. \tag{10}$$

Of all operators satisfying Eq. (9), this is the one that minimize Eq. (8). The projection filter has following advantages: (i) the characteristics of noise is considered; (ii) the error is directly evaluated in the original dipole layer space; (iii) the optimum approximation to each dipole layer distribution is obtained; (iv) a priori information of the dipole layer distribution is not required.

Although the projection filter criterion is natural, it seems that the condition Eq. (9) is too severe. If a small derivation of BA from P suppresses strongly the noise component in the restored signal, then it is possible to obtain a better restoration filter. A combined criterion, giving the parametric projection filter (PPF) [43], is

$$Minimize \quad J(B) = ||P - BA||^2 + \gamma E||B_n||^2 \tag{11}$$

The first term is the squared Schmidt norm. The scalar parameter $\gamma > 0$ in Eq. (11) controls the mutual weights of two error terms. The determination of the value of

parameter *gamma* is left to the subjective judgment of the user. The optimum choice for γ is described in the next section. The PPF, that satisfying Eq. (11), is given by [43]

$$B = A^*(AA^* + \gamma Q)^{-1}. \tag{12}$$

We have applied the parametric projection filter to the inverse problem described by Eq. (2). The parametric projection filter only uses the noise covariance, Q, while the parametric Wiener filter uses both the signal covariance, R, and the noise covariance, Q. In a clinical and experimental setting, the noise covariance Q may be estimated from data that is known to be source free, such as pre-stimulus data in evoked potentials [35]. The restoration filters and their evaluation functions are summarized in Table 1.

2.3 Parameter Estimation

The restoration filters have a free parameter that determines the restorative ability. The optimum parameters for each restoration filter should be determined by minimizing the relative error (RE) between the actual dipole layer distribution and the estimated dipole layer distribution as

$$RE = ||f - f_0||/||f||. \tag{13}$$

Unfortunately, the original dipole layer distribution, f, could not be obtained in actual situation. We have developed a criterion for determining the optimum parameter. The square error between f and f_0 is rewritten by following equation.

$$\begin{aligned} &||f - f_0||^2 = ||f - B(Af + n)||^2 \\ &= ||f - BAf||^2 + ||B_n||^2 + 2(B_n, f - BAf). \end{aligned} \tag{14}$$

By expectation for noise,

$$||f - BAf||^2 + E||B_n||^2 + 2E(Bn, f - BAf). \tag{15}$$

The last term in Eq. (15) can be approximated by zero because $E(n) = 0$. The first term in Eq. (15) represents the restorative error while the second term in Eq. (15) represents the amplitude of noise in the restored plane. Without knowing the original dipole layer distribution f, it is possible to directly evaluate the first term in Eq. (15). One possibility is to use the following procedure.

1. Compute the restoration f_0 using an initial value for γ, which should be relatively large to reduce the effect of additive noise on the coefficients.
2. Replace f by f_0 in Eq. (15) and calculate the following function:
$$J(\gamma) = ||f_0 - BAf_0||^2 + E||B_n||^2 \tag{16}$$
3. Obtain new optimum parameter γ_1 by minimizing Eq. (16).
4. Repeat 1.– 3. using new γ_1 until $||\gamma - \gamma_1||/||\gamma|| < e$ (e: the condition of convergence)

Then at least the order of magnitude of the function in Eq. (15) should be correct. Concretely, the initial value for γ can be selected when the second term of Eq. (16), which represents the amplitude of noise in the restored plane, is sufficiently small. The following computer simulation indicates that this procedure also provides the unique solution of γ despite of varying the initial value. This method is also applicable for other parametric inverse techniques such as the TSVD, the TKNV and the PPF.

2.4 Simulation Method

In our simulation, two dipole sources were used to represent two well-localized areas of brain electrical activity. The dipoles were oriented radially or tangentially to the sphere with varying distance between them and with varying eccentricity. For the radial dipole, the direction of the dipole moment is along the radius of the sphere. For the tangential dipole, the direction of the dipole is perpendicular to the radial dipole.

In the present study, due to the important cause of the smearing effect by the low conductivity of the skull, the head volume conductor was approximated using the inhomogeneous three-concentric-sphere model [44], as shown in Fig. 1. In this model, the radii of the brain, r_1, the skull, r_2, and the scalp, R, spheres were taken as 0.87, 0.92, and 1.0, respectively [24], [44]. The normalized conductivity of the scalp and the brain was taken as $\sigma = 1.0$, and that of the skull as $\sigma_s = 0.0125$. The potentials on the scalp and cortical surface, generated by current dipoles inside the brain, can be calculated by solving the forward problem from the dipole source to the scalp/cortical surface potential [24].

Various noises, such as uniform distribution of Gaussian white noise and edge-, center- and one side-concentrated non-uniform noise were added to the cal-

Table 1 Restoration filters and evaluation functions. V_γ, U_γ: matrices composed of γ singular vectors; S_γ: the diagonal matrix with γ singular values; I: the unit matrix; $Q = E[nn^*]$.

Inverse filter	Evaluation function in original image space	Evaluation function in observed image space	Restoration filter, B
TSVD	$\|\|f_0\|\|^2$	$\|\|Af_0 - \gamma\|\|^2$	$V_\gamma S_\gamma^+ U_\gamma^*$
TKNV	$\|\|f_0\|\|^2$	$\|\|Af_0 - \gamma\|\|^2$	$A^*(AA^* + \gamma I)^{-1}$
PPF	$\|\|BA - P\|\|^2 + \gamma E\|\|B_n\|\|^2$		$A^*(AA^* + \gamma Q)^{-1}$

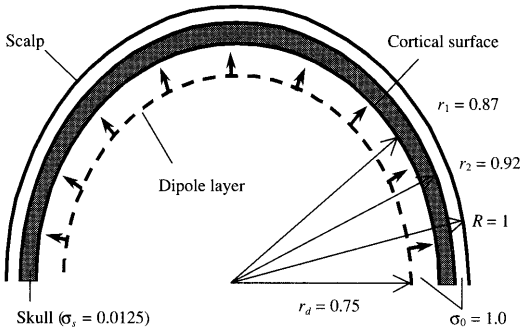

Fig. 1 Schematic illustration of the conductor-source model. The head is represented by an inhomogeneous concentric three-sphere volume conductor model with radii r_1, r_2, and R being 0.87, 0.92, and 1.0, respectively. Dipoles are uniformly distributed over a sphere. The potential distribution over the cortical surface at the radius of 0.87 is reconstructed from the dipole layer.

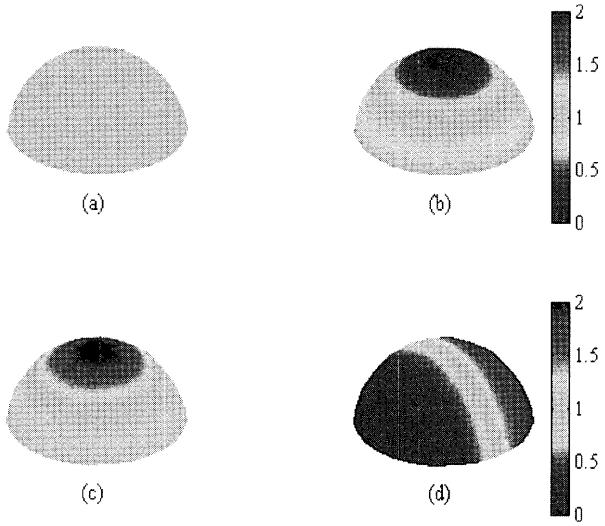

Fig. 2 Distributions of the diagonal of noise covariance over the space domain. Uniform distribution of (a) GWN and (b) edge-, (c) center- and (d) side-concentrated non-uniform distribution were used in the present computer simulation studies. The color scale corresponds to the absolute amplitude of the noise over the upper hemisphere.

culated scalp potential to simulate noise-contaminated measurements in the present computer simulation studies. Figure 2 shows the distributions of the diagonal of noise covariance over the space domain. The color scale corresponds to the absolute amplitude of the noise over the upper hemisphere. The dynamic range of three non-uniform noises was set to from 0.1 to 1.9 while that of Gaussian white noise was 1.0. The noise level (NL) is defined as the ratio between the norm of noise and that of the simulated scalp potential distribution as

$$NL = ||n||/||g|| \tag{17}$$

The performance of the proposed method was compared with that of TSVD and TKNV in the same conditions. Seven trials of each noise distributions were simulated and inverse estimations performed for each of seven sets of noise-contaminated scalp potential data. The results presented in Sect. 3 are averaged values over the ten sets of inverse solution. In each simulation, the standard deviation of the relative error was also evaluated over ten trials of data.

After the dipole layer strength was determined, the potential distribution over the cortical surface was reconstructed from the dipole layer by Eq. (3). On the other hand, the actual cortical potential can be directly calculated from the dipole sources [24]. The reconstructed cortical potential was then computed with the actual cortical potential to evaluate the performance of the inverse procedure. The RE, defined by

$$RE = ||h - h_0||/||h||, \tag{18}$$

is used to measure the similarity between the patterns of the cortical potential distribution and its estimated counterpart.

2.5 Human Experimentation

Human VEP experiments were carried out to examine the performance of the proposed restoration method. A healthy subject was studied in accordance with a protocol approved by the Institutional Review Board of the University of Illinois at Chicago. Visual stimuli were generated by the STIM system (Neuro Scan Labs, Inc.). 96-channel VEP signals referenced to right earlobe were amplified with a gain of 500 and band-pass filtered from 1 Hz to 200 Hz by Synamps (Neuro Scan Labs, Inc.), and were acquired at a sampling rate of 1 kHz by using SCAN 4.1 software (Neuro Scan Labs, Inc.). The electrode locations were measured using Polhemus Fastrack (Polhemus, Inc.) and best fitted on the spherical surface with unit radius. Half visual field pattern reversal check boards (black and white) with reversal interval of 0.5 sec served as visual stimuli and 400 reversals were recorded to obtain averaged VEP signals. The display had a total viewing angle of 14.3 degree by 11.1 degree, and the check size was set to be 175' by 135' expressed in arc minutes.

3. Results

3.1 Effects of Source Eccentricity

The following parameters were used in the present simulation studies: 1) the upper hemispherical dipole layer at the radius of 0.75, 2) 1280 radial dipoles uniformly distributed over this dipole layer, 3) 256 points of reconstruction over the cortical surface, and 4) the parameters of the three restoration filters were estimated by the method in Sect. 2.3.

Figure 3 shows an example of the cortical and scalp potentials calculated directly from two radial dipoles. The scalp potentials measured with 128 electrodes were

contaminated with 10% edge-concentrated noise. The color scale corresponds to the amplitude of the potential. The positions of two dipole sources, which represent two localized brain electrical activities, are given as follows:

$$(\pm r\sin(\pi/12), 0, r\cos(\pi/12)) \tag{19}$$

where r is the eccentricity of the two dipoles, and was set to 0.75. Note that the two poles in the cortical potential distribution (Fig. 3 (a)) are indistinguishable in the scalp potential distribution (Fig. 3 (b)).

Figure 4 shows the RE versus the eccentricity of dipoles in three inverse techniques. Two dipoles, located at the positions given by Eq. (19) with varying eccentricity r, were used as the sources. The number of electrodes on the scalp was set to 128. Four noise distributions as shown in Fig. 2 were added to the calculated scalp potential with 10% NL. Figure 4 indicates that the relative errors for superficial sources are larger than those for deep sources in every noise distribution. This is due to the effect of noise in the scalp potential, which was discussed in [24]. Especially, the relative errors were exponentially proportion to the eccentricity of sources, because high spatial resolution was required to reconstruct the cortical potential distribution for superficial sources. In the case of center-concentrated distribution of dipole as shown in Fig. 3, the proposed method was very effective for edge-concentrated non-uniform noise as shown in Fig. 2 (b). The results of the proposed method was better than that of the TSVD and the TKNV in the cases of the Gaussian white noise and one-side concentrated non-uniform noise and was similar to that of the TSVD and the TKNV in the case of center-concentrated distribution of noise covariance. The mean and maximum value of the standard deviation of ten trials was 0.016 and 0.045, respectively. The following simulations had the similar range of the values of the standard deviation of ten trials.

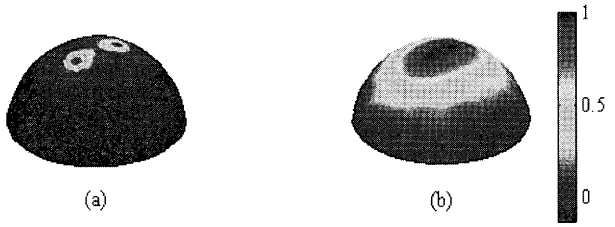

Fig. 3 One example of the cortical and scalp potentials. Two radial dipoles were located at Eq. (19) with the eccentricity of 0.75 and the angle of two dipoles was $\pi/6$. (a) The cortical potential map was constructed from 256 potential values over the cortical surface. (b) 128 electrodes were used for the scalp potential, which is contaminated with 10% edge-concentrated noise. The color scale corresponds to the amplitude of the potential.

3.2 Effects of Noise Levels

The relative errors were calculated with varying the NL (Fig. 5). The eccentricity was set to 0.60. The other parameters such as the positions of dipole sources, the number of electrodes, noise distributions, inverse methods and parameter estimation were the same as Fig. 4. The smaller the NL, the better the results. The results

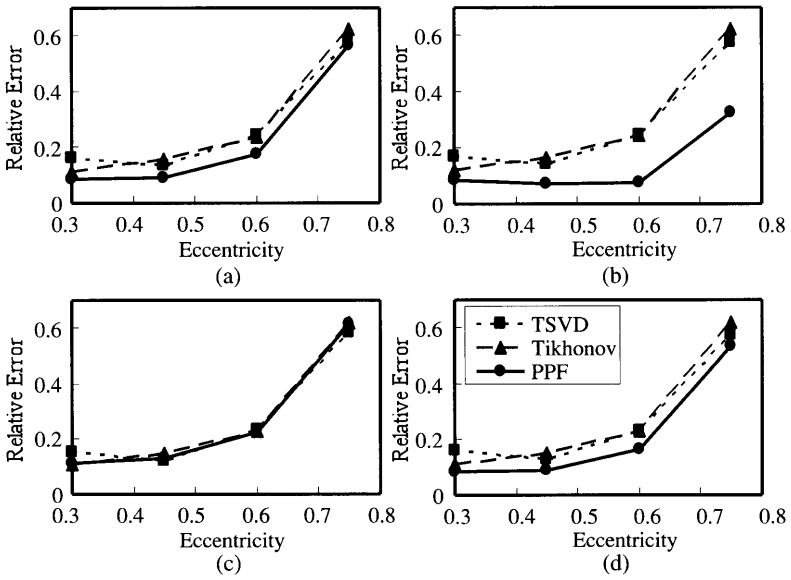

Fig. 4 Eccentricity vs. relative errors. Squares: TSVD; Triangles: TKNV; Circles: PPF. The eccentricity is defined by the distance from the center of sphere to the locations of dipole sources as shown in Eq. (19). The 10% NL of (a) GWN, (b) edge-, (c) center-, and (d) side-concentrated noise were added to the scalp potential. The number of scalp electrodes was set to 128.

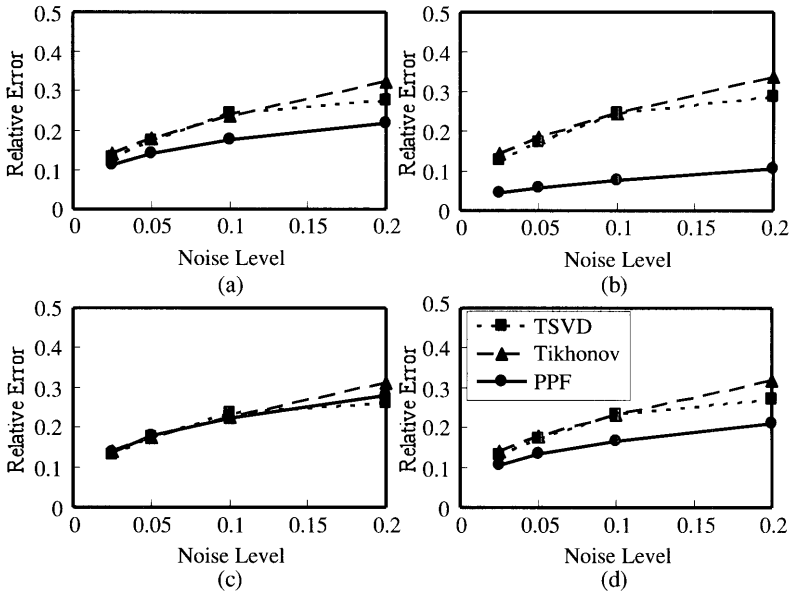

Fig. 5 Noise level vs. relative errors. Squares: TSVD; Triangles: TKNV; Circles: PPF. The noise level is defined as the ratio between the norm of signal and the norm of noise. The eccentricity of two dipole sources as shown in Eq. (19) was set to 0.60. (a) GWN, (b) edge-, (c) center-, and (d) side-concentrated noise were added to the scalp potential. The number of scalp electrodes was set to 128.

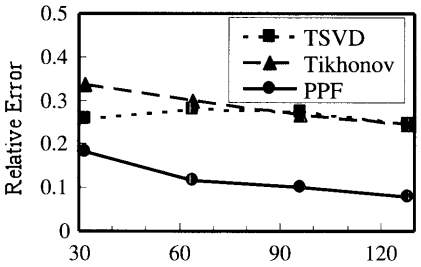

Fig. 6 Effects of electrode numbers. The eccentricity of dipole sources is 0.60. 10% edge-concentrated non-uniform noise was added to the scalp potentials with 128 electrodes.

of Fig. 5 indicate that for the edge-concentrated colored noise examined in this case, the proposed method provides an enhanced performance as compared with the TSVD and TKNV methods.

3.3 Effects of Electrode Numbers

The number of electrodes is also an important factor in cortical potential imaging because it limits the spatial sampling of the scalp potential. Figure 6 shows the effect of the number of electrode on the cortical potential imaging. The eccentricity of dipole source was set to 0.60 and the edge-concentrated non-uniform noise of 10% NL was added to the calculated scalp potential. 32, 64, 96, and 128 electrodes were simulated in the present study. In all cases, the result of the proposed method was better than that of the TSVD and the TKNV. Figure 7 shows an example of the inverse solution of the estimated cortical potential distribution.

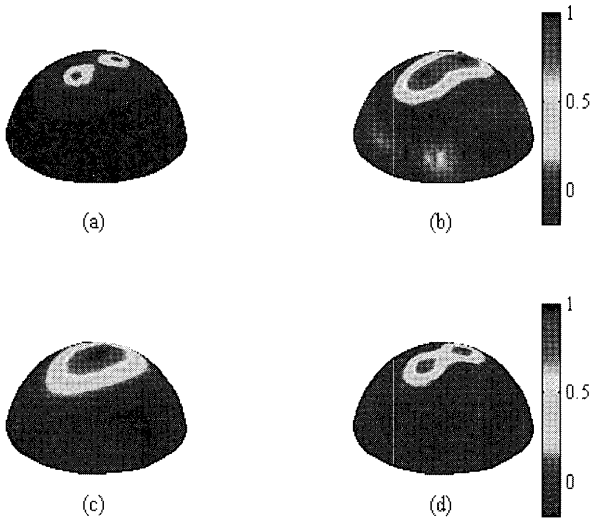

Fig. 7 One example of the estimated inverse solution of cortical potential imaging by means of the (b) TSVD, (c) TKNV and (d) PPF. (a) shows the actual cortical potential. Two radial dipoles were located at Eq. (19) with the eccentricity of 0.75 and the angle of two dipoles was $\pi/6$. A 10% edge-concentrated non-uniform noise was added to the scalp potential to simulate the noise-contaminated measurements. Note the improved performance of the PPF as compared with the TSVD and TKNV in this case.

The color scale corresponds to the amplitude of the potential. 10% edge-concentrated non-uniform noise was added to the scalp potential. The eccentricity was 0.75. It is shown that the proposed method (Fig. 7 (d)) provides an enhanced performance in reconstructing the two radial dipole source configuration as compared to the regular TSVD (Fig. 7 (b)) and TKNV (Fig. 7 (c))

methods.

3.4 Effects of Parameter γ

The parametric projection filter consists of a free parameter, γ. We have proposed a new parameter estimation method to determine this regularization parameter as shown in 2.3. In this section, we consider the effects of the parameter γ for restoration. Figure 8 (a) shows an example of the performance of the parametric projection filter in estimating the parameter γ. The relative error between the actual and the estimated cortical potentials is plotted against the parameter γ.

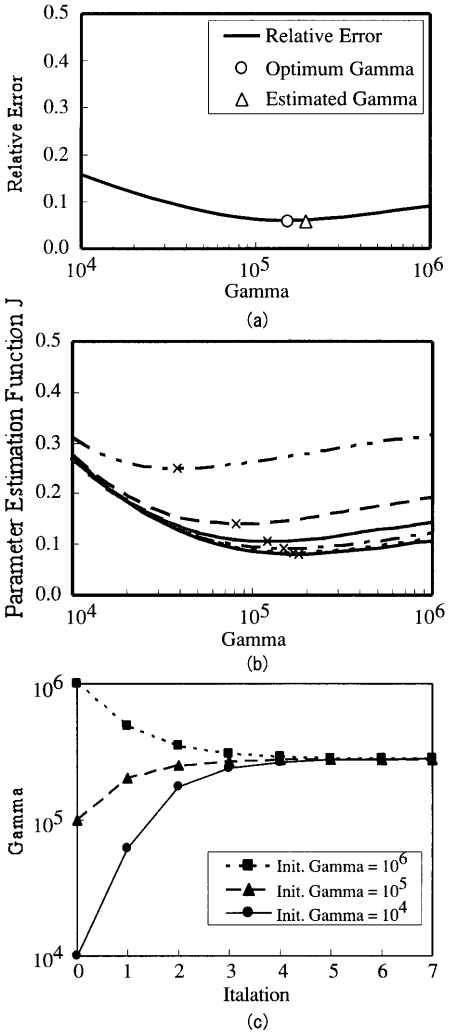

Fig. 8 Effects of parameter γ: (a) The RE between actual and estimated cortical potentials was shown against the parameter γ. The eccentricity of dipole sources is 0.45. 10% edge-concentrated non-uniform noise was added to the scalp potential with 128 electrodes. The circle indicates the minimum of the RE curve and the triangle indicates the RE using the estimated parameter by the method of Section 2.3. (b) The functions $J(\gamma)$ in Eq. (16) and their minimum (cross) are plotted against the parameter γ. (c) The estimated parameter γ in repetition. Three plots correspond to the initial value of 10^4, 10^5, and 10^6, respectively.

The eccentricity of dipole sources was 0.45. 10% edge-concentrated non-uniform noise was added to the scalp potential with 128 electrodes. The optimum parameter (circle) was calculated by the minimum of the RE curve between the actual and the estimated cortical potential while the estimated parameter (triangle) was calculated by the method of Section 2.3. Figure 8 (b) shows the evaluation functions of iterations in Eq. (16) that are normalized by $||f_0||$ and their minimum (cross). In the present simulation, the initial value of γ was 10^4. Figure 8 (c) shows the values of estimated parameter γ in repetition. Three plots correspond to the initial value of 10^4, 10^5, and 10^6, respectively. Whenever the initial value was set to any values, the estimated parameters converge to same value. We confirmed that the iteration number of 10 was enough to convergence in all simulations conducted. Though the estimated parameter was slightly different from the optimum parameter, the RE obtained by the estimated parameter was similar to that obtained by the optimum parameter. When the cortical potential was obtained using the estimated parameter, the relative error became worse 0.015 in average than that obtained using the optimum one.

Figure 9 shows an example of the effect of the parameter γ. The eccentricity of dipole sources was 0.75. 10% edge-concentrated non-uniform noise was added to the scalp potential with 128 electrodes. When the parameter was set to the small value, two dipole sources were identical while the estimated cortical potential became noisy. On the other hand, when the parameter was set to large value, we could not see the two-dipole

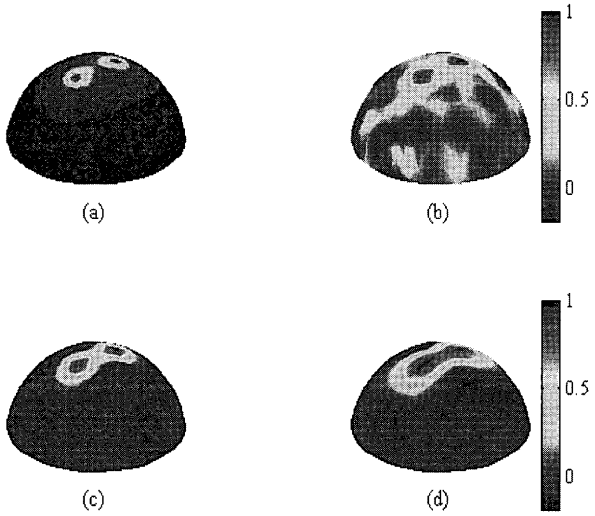

Fig. 9 On example of the effect of the parameter, γ: (a) the actual cortical potential, (b) the estimated cortical potential with 0.1 times of the optimum parameter, that was calculated with the minimum RE, (c) the estimated cortical potential with the optimum parameter, and (d) the estimated cortical potential with 10 times of the optimum parameter. The eccentricity of dipole sources is 0.75. 10% edge-concentrated non-uniform noise was added to the scalp potential with 128 electrodes.

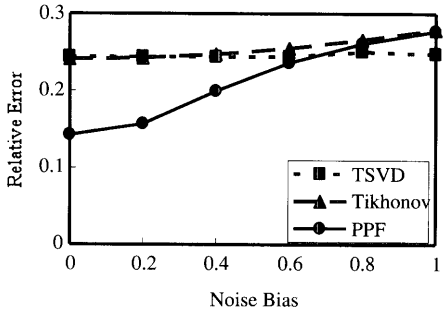

Fig. 10 Effect of estimation error in noise covariance Q. The noise bias, which was defined by an amplified Gaussian white noise, was added to Q in the PPF and the parameter estimation functions. The horizontal axis is the amplitude of the noise bias. The vertical axis is the RE between the actual and estimated cortical potential using the biased Q. The eccentricity of dipole sources is 0.75. 10% edge-concentrated non-uniform noise was added to the scalp potential with 128 electrodes.

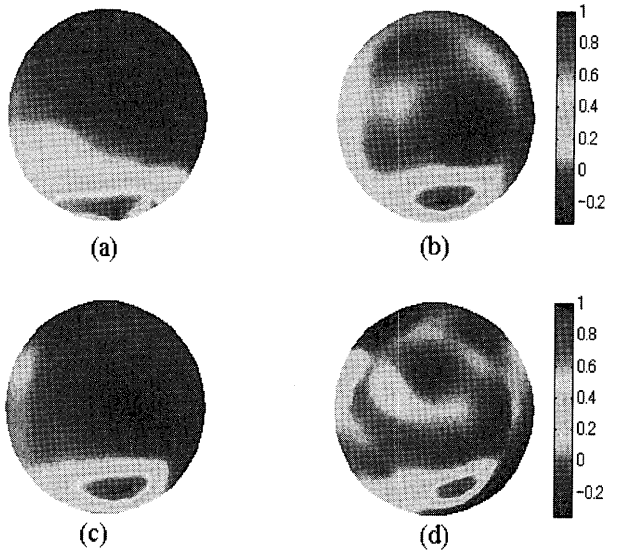

Fig. 11 Application of the restoration filters to cortical potential imaging of VEP induced by left visual stimuli in a human subject. (a) Normalized scalp potential map at P100 in response to the left visual stimuli. Normalized cortical potential maps estimated by the TSVD, TKNV, and PPF are shown in (b), (c), and (d), respectively.

sources while the noise was suppressed. The determination of the value of parameter γ depends on the application. If high spatial resolution is required, then γ should be set to small value.

3.5 Effects of Estimation Error in Noise Covariance

In actual situation, the noise covariance Q should be estimated in order to perform the parametric projection filter. The noise covariance Q can be calculated using the set of the noise. We examined the estimation error of Q (Fig. 10). The spatial distribution of noise that constructs Q was modified by adding the noise bias that was defined by the amplified Gaussian white noise. The inverse techniques using the modified Q were applied for the scalp potential that was contaminated with the unmodified Q. The horizontal axis shows the ratio between the noises and the noise bias. The vertical axis shows the relative error between the actual and the estimated cortical potential using the biased Q. The relative error of the proposed method became large by increasing the bias of Q while the relative errors of the TSVD and the TKNV were nearly constant. The relative error of the parametric projection filter was more sensitive for the Q that the TSVD and the TKNV in estimating the parameter γ because the equation of the parametric projection filter consists of Q. This result demonstrates that if the noise covariance is estimated accurately, the proposed method provides better results than the TSVD and TKNV.

3.6 Cortical Imaging of Human VEP

The pattern reversal VEP data at the P100 were analyzed by the restoration filters of the TSVD, TKNV, and PPF. Figure 11 shows an example of (a) the scalp potential map and the estimated cortical maps by (b) TSVD, (c) TKNV, and (d) PPF in a healthy subject. As shown in Fig. 11 (a) in response to the left visual stimuli, a dominant positive potential component was elicited with a widespread distribution on the bilateral scalp. However, the estimated cortical potential map reveals a dominant in the right visual cortex. Especially, the result of the PPF was much more localized than that of the TSVD and TKNV.

4. Discussion

Research progress in the past decade has established the high-resolution EEG methodologies for imaging brain electrical activity. The cortical imaging approaches are virtually applicable to any kind of brain source distribution (both localized and distributed). This is due to the generalized nature of the equivalent surface source models behind the cortical imaging techniques. These techniques should be useful particularly for localizing and imaging cortical sources. The cortical current imaging approach models directly the cortical sources using a distribution of current dipoles oriented normal to the cortical surface [10], [13]. While such current dipole layer modeling may correlate directly the scalp EEG recordings with the underlying cortical sources, the current dipole layer imaging is nonunique since different specifications of the current dipole distribution will lead to different solutions. On the other hand, cortical potential imaging estimates the electrical potential over the epicortical surface from scalp potentials. Since there are, in principle, no primary bioelectric sources between the scalp and epicortical surfaces, such approach is theoretically unique [30]. Cortical potential imaging is also sometimes called as downward

continuation [19], [20], [25]. While epicortical potential is not a primary source itself, it does reflect much spatial details on the underlying brain electric activity, especially cortical sources, due to the vicinity of the epicortical observation surface to the cortical sources.

Cortical potential imaging is not a non-unique inverse problem, but an ill-posed and underdetermined inverse problem. Noise plays an important role in cortical potential imaging, as in any other ill-posed inverse problem. Since every cortical potential imaging technique needs to seek the inverse of a transfer matrix, a small amount of noise existing in measurement may result in large errors in the cortical potential inverse solutions. So far, most cortical potential imaging techniques [16]–[27] deal with the effect of noise without considering noise covariance.

In the present study, we have investigated the performance of cortical potential imaging by considering noise covariance through the use of parametric projection filter. While sophisticated regularization methods have previously developed including both signal covariance and noise covariance [10]–[12], [14], [35], there is no, to our knowledge, comprehensive investigation on cortical potential imaging in the metric of noise, in which non-white noise is considered. The present study demonstrates that enhanced performance can be obtained in cortical potential imaging by considering the noise covariance.

Figures 4–7 show that the proposed method provides a good performance when the dipoles were located at the center of the head model and the noise was distributed around the edge. Moreover, the result of the proposed method is similar to the TSVD and TKNV, in which the information on the noise covariance is not considered, when the noise was concentrated at the center. The correlation coefficient between the cortical potentials in Fig. 3 (a) and the diagonal of Q as shown in Fig. 2 (a), (b), (c), and (d) was 0.026, -0.926, 0.966, and -0.092, respectively. The present results suggest that, the proposed method is effective for improving cortical potential imaging, under the condition of low correlation between signal and noise. The proposed method will have similar restorative ability to the regularization procedures without considering the information of noise covariance, under the condition of high correlation between signal and noise. Theoretically, the noise covariance Q of the Gaussian white noise is identical to the scaled unit operator I. So, the proposed method in Eq. (12) will be as same as the TKNV in Eq. (5), for Gaussian white noise. In the present simulation, the noise in Fig. 2 (a) was not exactly the Gaussian white noise because the size of noise is limited in finite values. Since the noise covariance Q was actually estimated from the computer-generated noise, the result of the proposed method is slightly better than that of the TKNV.

As the parameter estimation methods for conventional regularization procedures used in cortical potential imaging, such as TSVD and TKNV, the L-curve approach [45], zero-crossing approach [46], and minimum product approach [47] have been proposed. In these methods the noise is assumed to be Gaussian white noise. In the case of non-white noise, the parameter γ of the proposed method should be selected by considering the relationship between the signal and noise. This relationship means not only the signal to noise ratio but also the relative difference between the signal distribution and the noise distribution. The present parameter estimation method is directly derived from the aim of this study that minimizing the error between the original signal and the estimated signal as shown in Eq. (14). The present method has some error because we use the estimated signal instead of the original signal and we ignore the third term in Eq. (15). However, the parameter estimation error is found to be negligible, as shown in the present simulation results. The initial value for γ is required in the present algorithm. We have numerically tested that the proposed algorithm converges to the same value regardless of initial values selected, and think it is beyond the scope of the present paper to develop a theoretical frame explaining the new algorithm we proposed. Such theoretical development shall be addressed in the future investigations. The present algorithm for determining the regularization parameter may be applied to other inverse estimation procedures, such as the TSVD, TKNV, etc.

5. Conclusion

The cortical imaging method has a flexibility of implementation and no *ad hoc* assumption about the nature of the generators of the scalp potential is required. The method may have important applications to better our understanding of brain functions and in facilitating clinical diagnosis of neurological diseases. The present results suggest that the PPF is effective for the condition of low correlation between the signal and noise and that has similar restorative ability to the TKNV for the GWN and the condition of high correlation between the signal and noise. The new parameter estimation method provided appropriate generalization parameter of PPF for high-resolution and noise-suppressed cortical imaging. Further investigation using experimental data is necessary to fully validate the performance of PPF for cortical imaging.

Acknowledgements

The authors wish to thank Dr. Jie Lian for assistance in collecting the VEP data. This work was supported in part by NSF CAREER Award BES-9875344, Grant-In-Aid for Scientific Research from Japanese Society for the Promotion of Science No. 13480291, and NIH 1RO1EB00178.

References

[1] P. Nunez, Electric Field of the Brain, Oxford Univ. Press, London, 1981.
[2] M. Scherg and D. Von Cramon, "Two bilateral sources of the AEP as identified by a spatio-temporal dipole model," Electroenceph. Clin. Neurophysiol., vol.62, pp.32–44, 1985.
[3] B. He, T. Musha, Y. Okamoto, S. Homma, Y. Nakajima, and T. Sato, "Electrical dipole tracing in the brain by means of the boundary element method and its accuracy," IEEE Trans. Biomed. Eng., vol.BME-34, no.6, pp.406–414, 1987.
[4] J.C. Mosher, P.S. Lewis, and R.M. Leahy, "Multiple dipole modeling and localization from spatio-temporal MEG data," IEEE Trans. Biomed. Eng., vol.39, no.6, pp.541–557, 1992.
[5] B.N. Cuffin, "A method for localizing EEG sources in realistic head models," IEEE Trans. Biomed. Eng., vol.42, no.1, pp.68–71, 1995.
[6] S. Ueno and K. Iramina, "Modeling and source localization of MEG activities," Brain Topography, vol.3, pp.151–165, 1990.
[7] S. Iwaki and S. Ueno, "Weighted minimum-norm source estimation of magnetoencephalography utilizing the temporal information of the measured data," J. Appl. Phys., vol.83, pp.6441–6443, 1998.
[8] T. Musha and Y. Okamoto, "Forward and inverse problems of EEG dipole localization," Crit. Rev. Biol. Eng., vol.27, pp.189–239, 1999.
[9] Y. Kosugi, N. Uemoto, Y. Hayashi, and B. He, "Estimation of intracranial neural activities by means of regularized neural network inversion techniques," Neurological Research, vol.23, pp.435–446, 2001.
[10] A.M. Dale and M.I. Sereno, "Improved localization of cortical activity by combining EEG and MEG with MRI cortical surface reconstruction: A linear approach," J. Cognitive Neuroscience, vol.5, pp.162–176, 1993.
[11] J.W. Philips, R.M. Leahy, and J.C. Mosher, "MEG-based imaging of focal neuronal current sources," IEEE Trans. Med. Imaging, vol.16, no.3, pp.338–348, 1997.
[12] R.G. de Peralta Menendez and S.L.G. Andino, "Distributed source models: standard solutions and new developments," in Analysis of neurophysiological brain functioning, ed. C. Uhl, pp.176–201, Springer Verlag, 1998.
[13] F. Babiloni, F. Carducci, F. Cincotti, C. Del Gratta, G.M. Roberti, G.L. Romani, P.M. Rossini, and C. Babiloni, "Integration of high resolution EEG and functional magnetic resonance in the study of human movement-related potentials," Methods Inf. Med., vol.39, pp.179–182, 2000.
[14] J. Hori and B. He, "Equivalent dipole source imaging of brain electrical activity by means of parameteric projection filters," Annals of Biomedical Engineering, vol.29, pp.436–445, 2001.
[15] B. He, D. Yao, and J. Lian, "High resolution EEG: On the cortical equivalent dipole layer imaging," Clinical Neurophysiology, vol.113, pp.227–235, 2002.
[16] R. Sidman, M. Ford, G. Ramsey, and C. Schlichting, "Age-related features of the resting and P300 auditory evoked responses using the dipole localization method and cortical imaging technique," J. Neurosci. Meth., vol.33, pp.23–32, 1990.
[17] R. Kearfott, R. Sidman, D. Major, and C. Hill, "Numerical tests of a method for simulating electrical potential on the cortical surface," IEEE Trans. Biomed. Eng., vol.38, no.3, pp.294–299, 1991.
[18] R. Srebro, R.M. Oguz, K. Hughlett, and P.D. Purdy, "Estimating regional brain activity from evoked potential field on the scalp," IEEE Trans. Biomed. Eng., vol.40, no.6, pp.509–516, 1993.
[19] J. Le and A. Gevins, "Method to reduce blur distortion from EEG's using a realistic head model," IEEE Trans. Biomed. Eng., vol.40, no.6, pp.517–528, 1993.
[20] A. Gevins, J. Le, N.K. Martin, P. Brickett, J. Desmond, and B. Reutter, "High resolution EEG: 124-channel recording, spatial deblurring and MRI integration methods," Electroenceph. Clin. Neurophysiol., vol.90, pp.337–358, 1994.
[21] P. Nunez, R.B. Silibertein, P.J. Cdush, R.S. Wijesinghe, A.F. Westdrop, and R. Srinivasan, "A theoretical and experimental study of high resolution EEG based on surface Laplacian and cortical imaging," Electroenceph. Clin. Neurophysiol., vol.90, pp.40–57, 1994.
[22] B. He, Y. Yang, S. Pak, and Y. Ling, "Cortical source imaging from scalp electroencephalograms," Med. Biol. Eng. Comput., vol.34, suppl., pp.257–258, 1996.
[23] F. Babiloni, C. Babiloni, F. Carducci, L. Fattorini, C. Anello, P. Onorati, and A. Urbano, "High resolution EEG: A new model-dependent spatial deblurring method using a realistically-shaped MR-constructed subject's head model," Electroenceph. Clin. Neurophysiol., vol.102, pp.69–80, 1997.
[24] Y. Wang and B. He, "A computer simulation study of cortical imaging from scalp potentials," IEEE Trans. Biomed. Eng., vol.45, no.6, pp.724–735, 1998.
[25] G. Edlinger, P. Wach, and G. Pfurtscheller, "On the realization of an analytic high-resolution EEG," IEEE Trans. Biomed. Eng., vol.45, no.6, pp.736–745, 1998.
[26] B. He, Y. Wang, and D. Wu, "Estimating cortical potentials from scalp EEG's in a realistically shaped inhomogeneous head model," IEEE Trans. Biomed. Eng., vol.6, no.10, pp.1264–1268, 1999.
[27] B. He, J. Lian, K.M. Spencer, J. Dien, and E. Donchin, "A cortical potential imaging analysis of the P300 and novelty P3 components," Human Brain Mapping, vol.12, pp.120–130, 2001.
[28] V.L. Towle, S. Cohen, N. Alperin, K. Hoffmann, P. Cogen, J. Milton, R. Grzesczcuk, C. Pelizzari, I. Syed, and J-P. Spire, "Displaying electrocorticographic findings on gyral anatomy," Electroenceph. Clin. Neurophysiol., vol.94, pp.221–228, 1995.
[29] B. He, Z. Zhang, J. Lian, H. Sasaki, S. Wu, and V.L. Towle, "Boundary element method based cortical potential imaging of somatosensory evoked potentials using subjects' magnetic resonance images," Neuroimage, vol.16, pp.564–576, 2002.
[30] B. He, "Brain electric source imaging: Scalp Laplacian mapping and cortical imaging," Crit. Rev. Biomed. Eng., vol.27, pp.149–188, 1999.
[31] M. Hamalainen and R. Ilmoniemi, "Interpreting measured magnetic fields of the brain: Estimates of current distributions," Univ. Helsinki, Finland Tech. Rep. TKK-F-A559, 1984.
[32] J.Z. Wang, S.J. Williamson, and L. Kaufman, "Magnetic source images determined by a lead-field analysis: The unique minimum-norm least-squares estimation," IEEE Trans. Biomed. Eng., vol.39, no.7, pp.665–675, 1992.
[33] R.D. Pascual-Marqui and R. Biscay-Lirio, "Low resolution electromagnetic tomography: A new method for localizating electrical activity in the brain," Int. J. Psychophysiology, vol.18, pp.49–65, 1994.
[34] R.D. Pascual Marqui, "Review of methods for solving the EEG inverse problem," Int. J. Bioelectromagnetism, vol.1, no.1, pp.75–86, 1999.
[35] K. Sekihara and B. Scholz, "Average-intensity reconstruc-

tion and Wiener reconstruction of bioelectric current distribution based on its estimated covariance matrix," IEEE Trans. Biomed. Eng., vol.42, no.2, pp.149–157, 1995.
[36] E. Biglieri and K. Yao, "Some properties of SVD and their application to digital signal processing," Signal Process., vol.18, pp.227–289, 1989.
[37] Y.S. Shim and Z.H. Cho, "SVD pseudo-inversion image reconstruction," IEEE Trans. Acoust. Speech Signal Process., vol.ASSP-29, no.4, pp.904–909, 1984.
[38] B.J. Sullivan and B. Liu, "On the use of singular value decomposition and decimation in discrete-time band-limited signal extrapolation," IEEE Trans. Acoust. Speech Signal Process., vol.ASSP-32, no.6, pp.1201–1212, 1984.
[39] A.N. Tikhonov and V.Y. Arsenin, Solutions of ill-posed problems, Wiley, New York, 1977.
[40] B.R. Hunt, "The application of constrained least squares estimation to image reconstruction by digital filter," IEEE Trans. Comput., vol.C-22, no.9, pp.805–812, 1973.
[41] H. Ogawa and E. Oja, "Projection filter, Wiener filter, and Kahunen-Loeve subspaces in digital image processing," J. Math. Anal. Appl., vol.114, no.1, pp.37–51, 1987.
[42] H. Ogawa, "Projection filter regularization of ill-conditioned problem — Inverse problems in optics," SPIE, vol.808, pp.189–196, 1987.
[43] E. Oja and H. Ogawa, "Parametric projection filter for image and signal restoration," IEEE Trans. Acoust. Speech, Signal Process., vol.ASSP-34, no.6, pp.1643–1653, 1986.
[44] S. Rush and D.A. Driscoll, "EEG electrode sensitivity — An application of reciprocity," IEEE Trans. Biomed. Eng., vol.BME-16, no.1, pp.15–22, 1969.
[45] P.C. Hansen, "Analysis of discrete ill-posed problems by means of the L-curve," SIAM Rev., vol.34, pp.561–580, 1992.
[46] P.R. Johnston and R.M. Gulrajani, "A new method for regularization parameter determination in the inverse problem of electrocardiography," IEEE Trans. Biomed. Eng., vol.44, no.1, pp.19–39, 1997.
[47] J. Lian and B. He, "A minimum product method and its application to cortical imaging," Brain Topography, vol.13, pp.209–217, 2000.

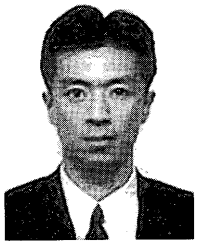

Junichi Hori received the B.E. and M.E. degrees in Information Engineering from Niigata University, Niigata, Japan, in 1986 and 1988, respectively. In 1996 he received the Ph.D. degree in Computer Science from the Tokyo Institute of Technology, Tokyo, Japan. In 1988 he joined the staff of the Department of Information Engineering, Niigata University, as a research associate. He is currently an associate Professor of Biocybernetics Department, Niigata University, Niigata, Japan. From 1999 to 2000, he was a Visiting Scholar in the Biomedical Functional Imaging and Computation Laboratory at the University of Illinois at Chicago. His research interests include inverse problem of physiological system, biomedical instrumentation, and biomedical signal processing and interpretation.

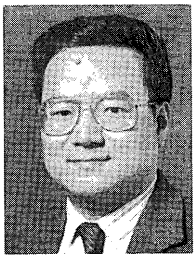

Bin He received his PhD degree in Bioelectrical Engineering with the highest honors from the Tokyo Institute of Technology, Japan, and completed his postdoctoral fellowship in Biomedical Engineering at Harvard University – MIT. After working as a Research Scientist at MIT, Dr. He joined the faculty of the University of Illinois at Chicago. Dr. He is currently an Associate Professor of Bioengineering, of Electrical and Computer Engineering, and of Computer Science, and the Director of Biomedical Functional Imaging and Computation Laboratory. His major research interests include modeling and imaging of bioelectric activity, neural engineering, cardiovascular engineering, and computational biomedicine. Dr. He is the recipient of NSF CAREER Award, American Heart Association Established Investigator Award, and the University of Illinois at Chicago College of Engineering Faculty Research Award. He has also been named a University Scholar by the President of the University of Illinois. Dr. He serves as the President of International Society of Bioelectromagnetism, and is an Associate Editor of IEEE Transactions on Biomedical Engineering and IEEE Transactions on Information Technology in Biomedicine.